# Determination of binary CO_2/H_2 adsorption isotherms and kinetics over porous organic cage CC3 via zero-length column technique

Jimmy D. L. Moreno[2] · Kyle Newport[3] · Ali A. Rownaghi[4] · Fateme Rezaei[1]

Abstract

Understanding the dynamics of mixed-gas adsorption is essential for industrial-scale adsorptive separations. Also, obtaining binary adsorption isotherms is essential to gain a better understanding of adsorbate-adsorbent interactions in multicomponent gas mixtures. Porous organic cages (POCs) are highly porous, crystalline materials, with a small average pore window that make them promising candidates for separation applications. In this work, we utilized zero-length column (ZLC) technique to not only determine the kinetics of CO_2/H_2 separation over CC3 but also obtain the binary adsorption isotherms. The ultracrystalline diffusivities of 1.49×10^{-4} and 8.31×10^{-5} cm^2.s^{-1} were estimated from the ZLC desorption profiles for unary CO_2 and H_2 gases at 293 K, respectively, whereas in binary CO_2/H_2 mixture, these diffusion values were reduced by 18 and 19 times, respectively. Moreover, our results indicated that the adsorption capacities estimated from binary runs diminished by approximately 36.0% and 33.6% for CO_2 and H_2, respectively, relative to the unary runs. The findings of this investigation highlight the importance of the ZLC technique in providing valuable insights on mixture adsorption equilibrium and dynamics without the need for tedious and complex experiments.
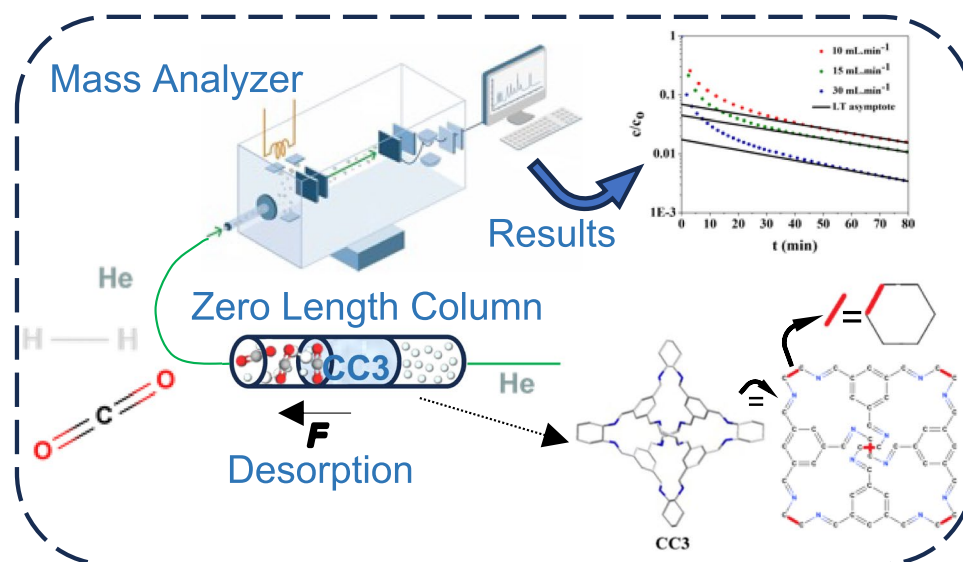
Keywords ZLC · POC · Diffusion · Binary adsorption isotherms · Kinetics

1 Introduction

Understanding multicomponent adsorption equilibria and dynamics is critical in developing highly efficient adsorptive separation systems [19, 21]. The insight into

multicomponent separation also allows for selecting an appropriate adsorbent for a particular process. It is a common practice to extract mixture equilibrium data from unary adsorption isotherms using the ideal adsorption solution theory (IAST), however, unary gas adsorption models cannot accurately predict binary adsorption due to non-ideal gasses, adsorbate–adsorbate interactions, and competitive/cooperative adsorption on the adsorbent surface [24]. For example, while CO_2/H_2 mixture is not difficult to separate, the presence of each gas alters the kinetic properties of another due to significant gas–gas interactions in the bulk phase, with smaller gas H_2, limiting the diffusivity of larger gas CO_2 [1, 20].

Producing binary adsorption isotherms is a time-consuming and tedious process. Various methods, such as breakthrough, volumetric, gravimetric, desorption, and specialty methods have been reported for this purpose [24]. Most of these techniques require large amounts of adsorbent, which results in large temperature fluctuations, thereby compromising the accuracy of generated data. Zero-length column (ZLC), as one of the desorption methods, is a straightforward and versatile technique for measuring not only intraparticle and/or intracrystalline diffusivities in microporous adsorbents, but also for obtaining equilibrium data and adsorption capacities [4, 11]. This method relies on exposing a small amount of adsorbent to a diluted feed at low flow rates. Due to the significantly short column length and small adsorbent mass, the heat effects and pressure drop are usually neglected, and thus the reliability of the ZLC data in determining adsorption equilibria and dynamics is usually high [12, 13, 17].

Among various adsorbent materials investigated for gas separation, porous organic cages (POCs) have recently emerged as popular candidates on the basis of their intrinsic guest-accessible cavities. Despite this, there exists limited understanding of their adsorption potential for energy-intensive separation processes. In particular, the POC CC3-R possesses intrinsic cavities that have four windows towards adjacent cages with a faceted octahedral crystalline structure, providing a large uniform pore structure, which makes it an ideal candidate for gas separation [8, 20].

In this study, we investigated CO_2/H_2 separation behavior of CC3-R using the ZLC technique. Specifically, we aimed at determining kinetic behavior and obtaining binary adsorption isotherms via ZLC experiments. Although most materials do not exhibit high affinity towards H_2, it is important to note the changes in kinetics behavior of H_2 in the presence of larger gases with high affinity toward adsorbent surface, such as CO_2. We systematically performed ZLC experiments with pure and binary mixtures of various compositions and flow rates along with blank runs to determine unary and binary diffusivities, Henry's constants, and ZLC parameters

for CO_2, H_2 and their binary mixtures from the ZLC desorption profiles at 90 °C.

2 Experimental section

2.1 CC3-R synthesis and characterization

The CC3-R POC was synthesized using a batch synthesis method, as reported by Briggs et al. [8]. Briefly, a solution of homochiral trans-CHDA (1R,2R-1,2-diaminocyclohexane) in dichloromethane (DCM) was gently layered onto a suspension of 1,3,5-triformylbenzene (TFB) in DCM, containing trifluoroacetic acid (TFA) over 5 days. The mixture was then dried at 80 °C in a vacuum oven and the resultant POC was collected after 6 h. All the chemicals used in the synthesis of CC3-R including TFB, DCM, TFA, and homochiral trans-CHDA were purchased from Sigma Aldrich, whereas CO_2, H_2, and $40\%CO_2/H_2$ gases with ultra-high purity were all obtained from Airgas.

The textural properties of the synthesized CC3-R powder were analyzed by N_2 physisorption at 77 K on a Micromeritics 3Flex gas analyzer. The sample was first degassed at 90 °C for 6 h at a ramp rate of 10 °C.min^{-1}. From the isotherms, the surface area and pore size distribution (PSD) were calculated using the Brunauer-Emmet-Teller (BET) and non-local density functional theory (NLDFT) methods, respectively [10].

2.2 Volumetric adsorption isotherms measurements

The volumetric CO_2 and H_2 adsorption isotherms were collected on a Micromeritics 3Flex from 0–1 bar, at 25, 35, and 55 °C to estimate the heats of adsorption using the Clausius Clapeyron method [15]. The sample in the powder form was degassed at 90 °C for 6 h prior to the adsorption isotherms measurements. Additionally, the CO_2/H_2 selectivity values were calculated from the unary adsorption isotherms using the IAST method [10].

2.3 ZLC experiments

In essence, the core of ZLC experimental procedure involved exposing the sample to a known mixture of gases, including the adsorbate(s) and an inert carrier gas (He), followed by switching the feed flow to the purge gas once equilibrium is attained, while recording the column outlet via a BelMass mass spectrometer. For a typical run, approximately 4.0 mg of agglomerated (shaped beads) POC was placed between two sintered discs in a 1/8-inch Swagelok union to ensure proper confinement within the ZLC column. The schematic of the ZLC setup is provided in our previous paper [14]. Degassing of the POC

was performed inside the ZLC column for 6 h at 90 °C under a He flow of 2 mL.min^{-1}. After which, the adsorbent was exposed to 2 mL.min^{-1} of either CO_2 and H_2, or CO_2/H_2 for 1–2 h at 25 °C until equilibrium was achieved. Subsequently, desorption step was started under varying He purge flow. The experiments were carried out using four feed compositions either diluted or undiluted in He (pure gas, A% of CO_2 or H_2 in He, where A is 10, 25 and 50 vol%) and three feed flow rates (10, 15, 30 mL.min^{-1}). The gas dilution was achieved using a mixing coil, which was placed approximately 90 cm prior to the inlet, providing sufficient time for the gases to mix before entering the column. The same experimental conditions were used for both unary and binary gas feed runs. The initial concentration of the binary mixture was 40% CO_2/H_2, resulting in the following CO_2/H_2 feed compositions (vol%) after dilution in He: 30/20, 15/10, and 6/4. Furthermore, blank runs (without adsorbent material inside the ZLC column), were conducted under the same configurations to obtain the natural response of each species in the column and to calculate the dead volume, V_g, an important parameter for the models.

2.4 Modeling section

2.4.1 Traditional analysis of diffusion model

Due to the short length of the ZLC column (approximately 9 mm) and the small inner diameter, the relative axial dispersion can be considered significant, implying that the system might effectively be treated as fully mixed. Thus, the mass balance can be described as follows:

$$V_s \frac{d\overline{q}}{dt} + V_f \frac{dC}{dt} + FC = 0 \tag{1}$$

Here, C and $\overline{q}$ represent the average concentration of the adsorbate in the fluid and adsorbed phases, respectively, V_s and V_f are the volume of the column occupied by the solid and fluid phases, respectively, and F is the volumetric flow rate.

For a diffusion model in micropores, the desorption profiles can be derived from Fick's Law of diffusion, assuming that the adsorbent particles are spherical with a radius of r_c, the intracrystalline diffusion of D_c – as the rate-limiting mass transfer step – and the dimensionless Henry's Law constant of H, related to linear equilibrium isotherms. An analytical solution for this system is given by [7]:

$$\frac{C}{C_0} = \sum_{n=1}^{\infty} \frac{2L}{[\beta_n^2 + L(L-1)]} exp\left(\frac{-\beta_n^2 D_c}{r_c^2} t\right) \tag{2}$$

where C_0 is inlet concentration and β_n is obtained as the roots of:

$$\beta_n cot\beta_n + L - 1 - \gamma\beta_n^2 = 0 \tag{3}$$

with $L = \frac{Fr_c^2}{3HV_sD_c}$ (4)

and $\gamma = \frac{V_f}{3HV_s}$ (5)

The non-dimensional parameter L is defined as the ratio between the diffusion time constant D_c/r_c^2 and the convective desorption time constant F/HV_s, while γ is a ratio that relates the fluid phase to the solid phase accumulation. It indicates the extent to which the system deviates from equilibrium-controlled dominance, [22] as there are cases where desorption can be controlled by a combination of internal diffusion effects and surface resistance [23]. In cases where significant surface resistance to mass transfer exists, the previous equations remain unchanged except for Eq. (4), where L becomes L', an apparent ratio between the time constants, given by the following equation:

$$\frac{1}{L'} = \frac{1}{L} + \frac{D_c}{kr_c} = \frac{1}{\gamma}\left(\frac{D_c}{r_c^2}\right) + \frac{D_c}{kr_c} \tag{6}$$

From Eq. (6), a plot of $1/L'$ vs. $1/F$ can be made, yielding a straight line with a slope of F/L and a y-intercept of D_c/kr_c, where k is the surface mass transfer coefficient. If it is permissible to neglect surface resistance, the line will pass through the Cartesian origin (or very close to it with an insignificant error).

2.4.2 Linear equilibrium model

When considering linear equilibrium, constant flow rate, and initial conditions $(t = 0, q = q_0 = HC_0)$, integrating Eq. (1) yields the following solution:

$$\frac{C}{C_0} = exp\left(\frac{-Ft}{HV_s + V_g}\right) \tag{7}$$

For weakly-adsorbed species, the value of HV_s is of the same order of magnitude as the dead volume, V_g. However, for strongly-adsorbed species, the dimensionless Henry constant may be larger, and the dead volume can be neglected ($HV_s \gg V_g$). Thus, H can be directly obtained from the slope, $-F/(HV_s + V_g)$, as a resulting line when plotting $ln(C/C_0)$ by the product Ft, or simply by time, $-1/(HV_s + V_g)$.

2.4.3 Nonlinear equilibrium model for single and binary isotherms

When moving away from the Henry's Law region, the equilibrium isotherm can be approximated by the Langmuir isotherm model. Again, considering equilibrium

conditions and integrating Eq. (1) with initial conditions $\left(t = 0, C = C_0\right)$, the solution is as the following:

$$ln\left(\frac{C}{C_0}\right) = \frac{-Ft}{HV_s + V_g} - \frac{HV_s}{HV_s + V_g}\left[\frac{1}{1 + bC} + \frac{1}{1 + bC_0} + ln\left(\frac{1 + bC_0}{1 + bC}\right)\right] \quad (8)$$

At sufficiently long times $(C \to 0)$, the graph of $ln(C/C_0)$ vs. Ft, obtained from the collected desorption curves, approaches a linear asymptote as the response. The linearity of desorption results in diluted concentration regions is independent of the adopted equilibrium isotherm model, whether linear or nonlinear since the slope remains as $-F/\left(HV_s + V_g\right)$. Therefore, the Henry's constant can be obtained from the slope of the asymptote at long times and continues to be used for estimating the diffusivity values and the correction factors.

After obtaining the desorption profiles and making the necessary corrections at long times, the adsorbed phase concentration can be determined from the experimental data. This is accomplished by integrating Eq. (1), from $t = 0$, when high adsorbate concentrations are present, to long-time $(t \to \infty)$, where concentrations become very low. Thus, the equilibrium concentrations obtained from the ZLC desorption profiles for individually saturated species and binary mixtures are given by Eqs. (9) and (10), respectively, where q^* is the equilibrium concentration of the adsorbed phase, and subscripts A and B refer to specific chemical species in the mixture [2, 3]:

$$q^* = \frac{FC}{V_s}\int_t^\infty \frac{y}{1 - y}dt - \frac{V_g\,C}{V_s}.y \quad (9)$$

$$q_A^* = \frac{FC}{V_s}\int_0^\infty \frac{y_A}{1 - y_A - y_B}dt - \frac{V_g\,C}{V_s}.y_A \quad (10)$$

With the concentrations $q_A^*(t)$ and $q_B^*(t)$ as functions of the partial pressures $p_A(t)$ and $p_B(t)$, it is possible to obtain the separation factor, α, as a function of time [2]:

$$\alpha = \left(\frac{q_A^*}{p_A}\right)\left(\frac{p_B}{q_B^*}\right) \quad (11)$$

The chosen model for fitting the experimental equilibrium data was the Dual-Site Langmuir (DSL) model since, when the adsorptive affinities of two adsorbates are significantly different, desorption typically occurs in two distinct steps. The "weaker" component is initially removed with each small change in the fluid phase concentration, and then the "stronger" component desorbs, similar to the single-component system [2]. The respective equations for the model are as follows:

$$q^* = \frac{b_1 q_{s1}p}{1 + b_1 p} + \frac{b_2 q_{s2}p}{1 + b_2 p} \quad (12)$$

$$q_A^* = \frac{b_{1A}q_{s1}p_A}{1 + b_{1A}p_A + b_{1B}p_B} + \frac{b_{2A}q_{s2}p_A}{1 + b_{1A}p_A + b_{1B}p_B} \quad (13)$$

where b_1, q_{s1}, and b_2, q_{s2} are representative parameters of active sites 1 and 2, respectively. Thus, the first terms in Eqs. (12) and (13) supposedly represent adsorption on "strong" sites within the super cages, whereas the second terms represent adsorption on "weak" sites.

3 Results and discussion

3.1 Analysis of blank tests and ZLC profiles

Figure 1 displays the blank desorption profiles for CO_2 and H_2 at different flow rates (10, 15, 30 mL.min^{-1}) and concentrations (100 and 10 vol% in He). Firstly, it is important to highlight that, in both initial concentration regions, the three desorption curves intercept at approximately the same common point, although it is more common to observe a shared region rather than a specific node [5]. These are fundamental benchmarks which indicate that the experimental conditions of the apparatus result in accurate data that corroborate well with the theoretical models. The formation of nodes stems from the variation in the ZLC parameter, L, derived from different desorption curves, which can be adjusted by changing the volumetric flow rate, F, or the equilibrium constant, H, in the model.

Moreover, it is clear from Fig. 1a that the profiles of pure CO_2 desorption exhibit greater curvature, almost linear as expected, in the region of diluted concentration, which can be defined at below 12% of relative concentration (C/C_0). Regarding the H_2 profiles in Fig. 1c, the interception point occurs faster than that for CO_2 with smaller slopes at the same relative concentration. The interception point of the pure CO_2 desorption curves occurs earlier and at a higher relative concentration compared to the curves at lower initial concentrations. The interception point indicates that the behavior of the ZLC system is consistent with expectations when varying the initial concentration. Furthermore, regarding the analysis of different initial concentrations, it is noteworthy that the curve at 15 mL.min^{-1} approaches the curve at 30 mL.min^{-1} for pure CO_2 (Fig. 1a), while the opposite occurs for diluted concentrations in Fig. 1b, where the profile at 15 mL.min^{-1} approaches the curve at 10 mL.min^{-1}. Based on these observations, it can be stated that, in these configurations, the ZLC system is well-adjusted, and the mass spectrometer is properly calibrated, and its signals are accurately measured according

Fig. 1 Blank ZLC profiles of CO_2 at 90 °C with (**a**) pure concentration ($C_0 = 100\%$) and (**b**) 10% of initial concentration diluted in He, and (**c**) blank desorption profiles of pure H_2 at the same temperature
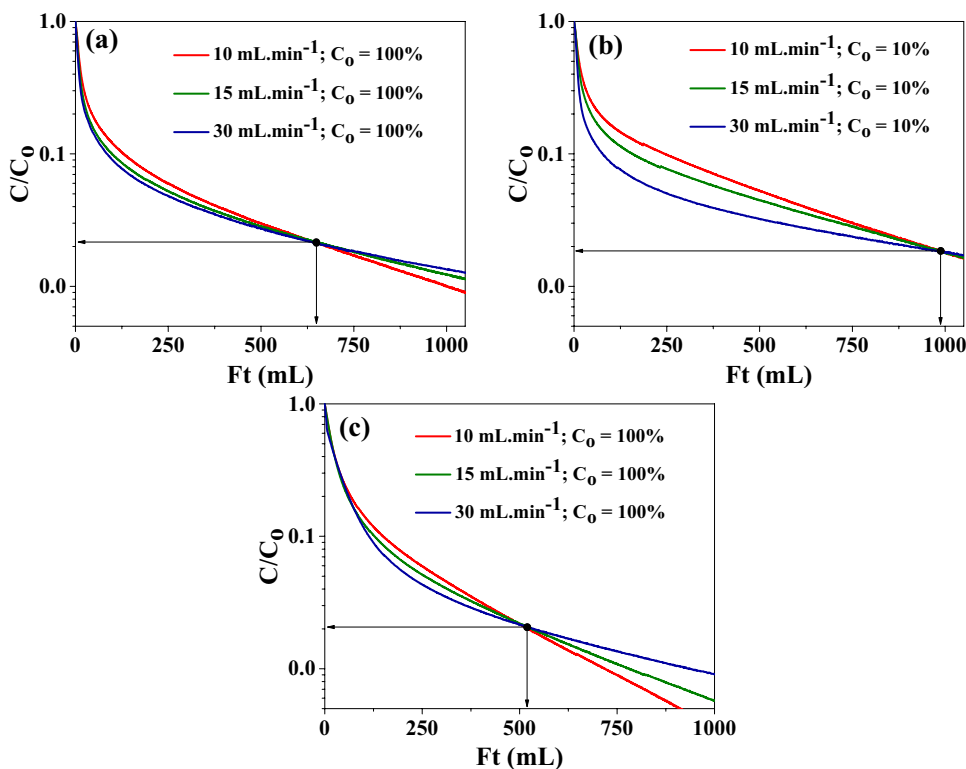
to the hypotheses described and discussed previously (see Section 2.4).

Proper analysis of the ZLC profiles requires a careful assessment of the dead volume from blank runs. As can be observed from Fig. 2, the region with relative concentrations from 0.5 to 1 exhibited linearity for both CO_2 and H_2, however, there was a dependence of the response on the feed flow rate. Nevertheless, across all runs, the slopes of the profiles converged to -0.023. This convergence was determined by considering the deviation values based on the steeper slope, obtained from the H_2 desorption at a 10 mL.min^{-1} flow rate with a 10% initial concentration [1, 2]. From these, the dead volume V_g was estimated to be 0.19 mL.

Figure 3a shows selected CO_2 desorption profiles at different flow rates and with 50% initial concentration in He. Unlike what was observed in the blank runs (Fig. 1), the three curves did not overlap at the same node or even in the same desorption region. Before arguing properly about which of the profiles was incorrectly measured by the mass spectrometer considering the fine tuning of the ZLC system, the curvature of the desorption profiles provides a hint. By carefully observing the region of low relative concentrations, such as below 4% for example, it is easier to notice that the 15 mL.min^{-1} profile exhibits greater curvature than the other two flow rates, even after applying the correction factor. This becomes more noticeable from point A onwards, comparing the 15 and 30 mL.min^{-1} profiles, and from point B backwards, comparing the 15 and 10 mL.min^{-1} profiles.

Fig. 2 Dead volume calculations from the ZLC blank runs for (**a**) CO_2 in two different initial concentrations (pure and 10% diluted in He) and (**b**) pure H_2
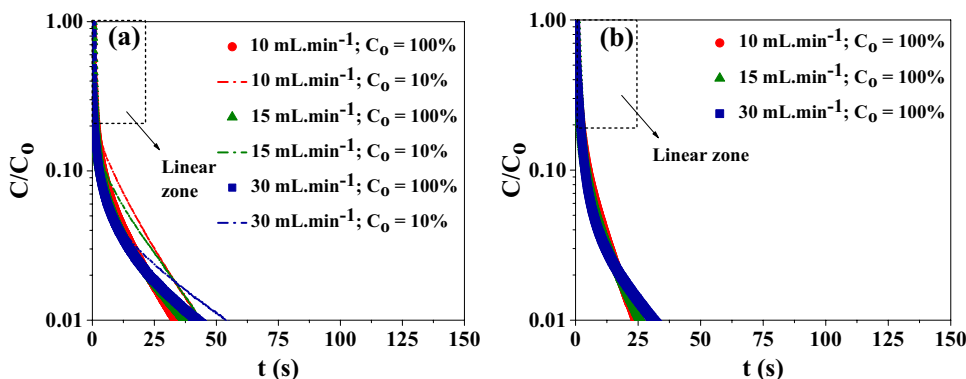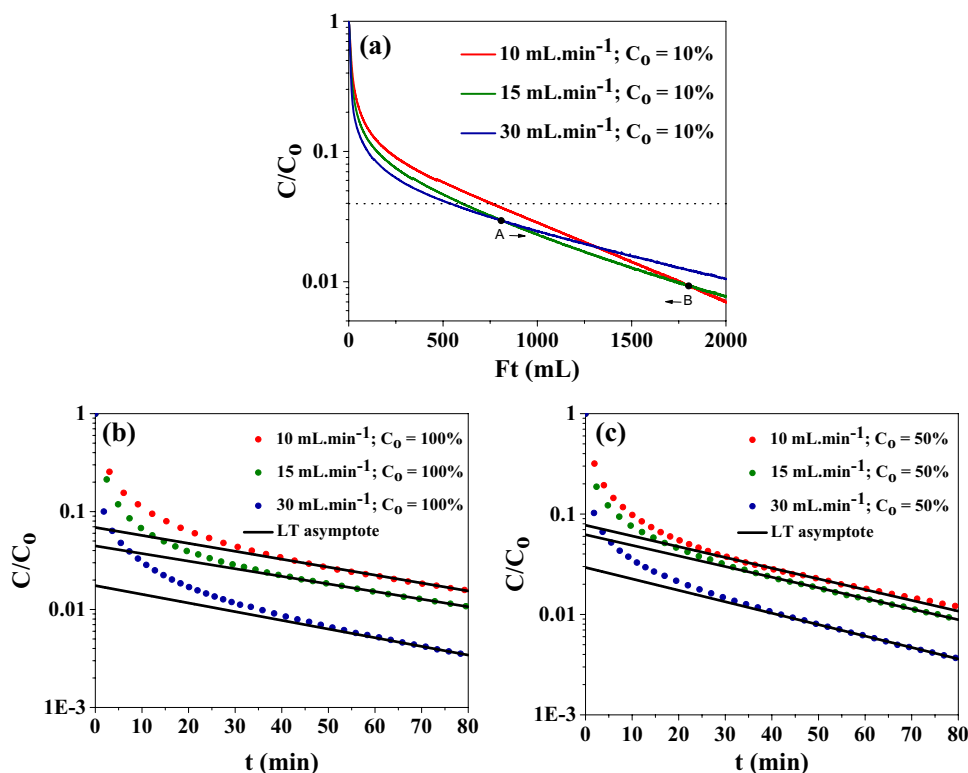
Fig. 3 Experimental ZLC desorption profiles for runs with initial concentrations of (**a**) 10% CO_2/H_2, (**b**) 100% CO_2, and (**c**) 50% CO_2/H_2, all at 90 °C

In many systems with highly diluted conditions ($< 1\%$), diffusivity tends toward the limit of "zero adsorbed phase loading". In other words, in the final region of desorption curves obtained by the ZLC system (extremely diluted zones), the rate of diffusion should be equivalent to the coefficient of self-diffusion and to that of a single adsorbent particle, the Maxwell–Stefan diffusivity [18]. In this configuration, mathematical models for mass transport combine the rate of diffusion with correction factors [6]. These corrections can be calculated from the slope of the isotherm and the secant of the isotherm from the Cartesian origin. This secant is also a linear relationship between the concentrations of the adsorbed phase ($\bar{q}$) and the adsorbate in the fluid phase (C). Nonetheless, considering that the determination of correction factors relies on obtaining the asymptotes at long times of desorption and that it depends on acquiring accurate data and their correct manipulation, the mathematically most appropriate way to determine which flow rate provided the least suitable data is by observing the slope coefficients of the asymptotes themselves. Regardless of whether the obtained correction factors are the best, the most reliable data generate asymptote slopes that tend to converge, provided that these factors have been calculated using the same methodology [6].

Figure 3b-c presents the asymptotes for the three flow rates after applying the correction. The fitting performed as a correction for the desorption curves of pure CO_2 (Fig. 3b) and 50% dilution curves (Fig. 3c) are assumed to be good

enough. The slope values were -0.019 and -0.020 for 10 and 30 mL.min⁻¹ at $C_0 = 100\%$, respectively, whereas at $C_0 = 50\%$ they were estimated to be -0.026 and -0.025. Therefore, the verification of the interception points of desorption curves from two flow rates and at the same concentration is conventionally performed only after applying data correction and after observing the slope of the asymptotes at diluted concentrations. In this case, the slopes for 15 mL.min⁻¹ in both initial concentrations were -0.021 and -0.026 for Fig. 3b-c, respectively.

This procedure serves as a form of validation for establishing the credibility of the raw data. Without it, the likelihood of these points coinciding within the same region of intersection is minimal, regardless of the data's quality assessment. Otherwise, it is very probable that the used technique needs more adjustments. While not a critical issue, it is important to note there are two main aspects regarding the use of ZLC systems that lead to nonlinear isotherms: the first is when dealing with strongly adsorbed components, and the second is when there are weak detection signals. The second aspect must be solved by increasing the concentration of the fluid phase in an attempt to obtain more and better equilibrium isotherm data [6, 11]. These issues are particularly prominent in Type I isotherms due to the exponential decay in desorption step at long times, if the detector is sensitive enough, resulting in an infinite shift down of the asymptote and a higher curvature in the initial region (which hinders the determination of kinetic parameters due to the lack of

required linearity for model application). Therefore, it is crucial to perform ZLC experiments with at least two feed flow rates at the same concentration to verify the linearity conditions of the proposed models. This avoids the introduction of significant uncertainties in diffusivity estimation, especially when the parameter L is small [6].

Hence, the nodes obtained from only two different flow rates can be considered reliable, as corroborated by the literature [4, 11], and as shown in Figs. 3b-c and 4a-c. Besides that, in this study all 15 mL.min^{-1} flow rate runs were performed consecutively on the same day. It is likely that the mass spectrometer was affected by a variation in electrical current due to preventive maintenance carried out in the facility building on that specific day. Another factor that can influence the reading of the mass spectrometer is a sudden change in ambient temperature at any point during the experiment. All experiments at 15 mL/min^{-1} were satisfactorily repeated, as seen in Fig. 4b and d, to estimate the kinetic parameters with greater precision, which is the main reason for choosing three different flow rates instead of just two.

In Fig. 4a-b, the interception points of the desorption curves at $C_0 = 10\%$ occur later and at a higher relative concentration than the curves at $C_0 = 100\%$. This is because the lower the concentration of the adsorbate during the column saturation step and the lower the feed flow rate, the greater the amount adsorbed by the adsorbent. This can be inferred based only on the curves from the blank runs under the same conditions, where the relative positioning of the nodes logically follows an inverse trend (see Fig. 1). Another relevant cause is the verification of the same curvature trend observed and discussed with the blank experiments when modifying the initial concentration. This observation is also evident in the H_2 desorption profiles (Fig. 4c-d), supporting the hypothesis of a reliable experimental setup, at least for individual experimental runs. Therefore, the ZLC system in this study was confirmed to be well configured to operate both with and without loaded POC in the column.

Figure 5 shows desorption profiles of unary CO_2 and binary CO_2/H_2 systems. Evaluation of unary/binary desorption profiles provides another valuable means to check the response of the ZLC system. As expected, the binary profiles of each adsorbate molecule are above of unary curves [2]. In these cases, it is essential to consider the purport of relative concentrations denomination for each adsorbate. While Fig. 5 could suggest that the POC adsorbs more CO_2 in the single-component system than in the binary system, or even that it adsorbs more H_2 than CO_2 in each system, such conclusions can only be drawn by examining the integral area between the desorption profiles of each system and their respective blank run profiles. Both validation forms of ZLC operation should match, for each adsorbate the slope analyses of single desorption profile and the unary/binary comparison of desorption profiles. Otherwise, it is a great indicative that the operation of the system is not reaching the minimum requirements to provide a desirable result.

Fig. 4 Experimental ZLC profiles for runs with initial concentrations of (**a**) 100% CO_2, (**b**) 10% CO_2/H_2, (**c**) 100% H_2 with two flow rates, and (**d**) 100% H_2 with three flow rates, all at 90 °C
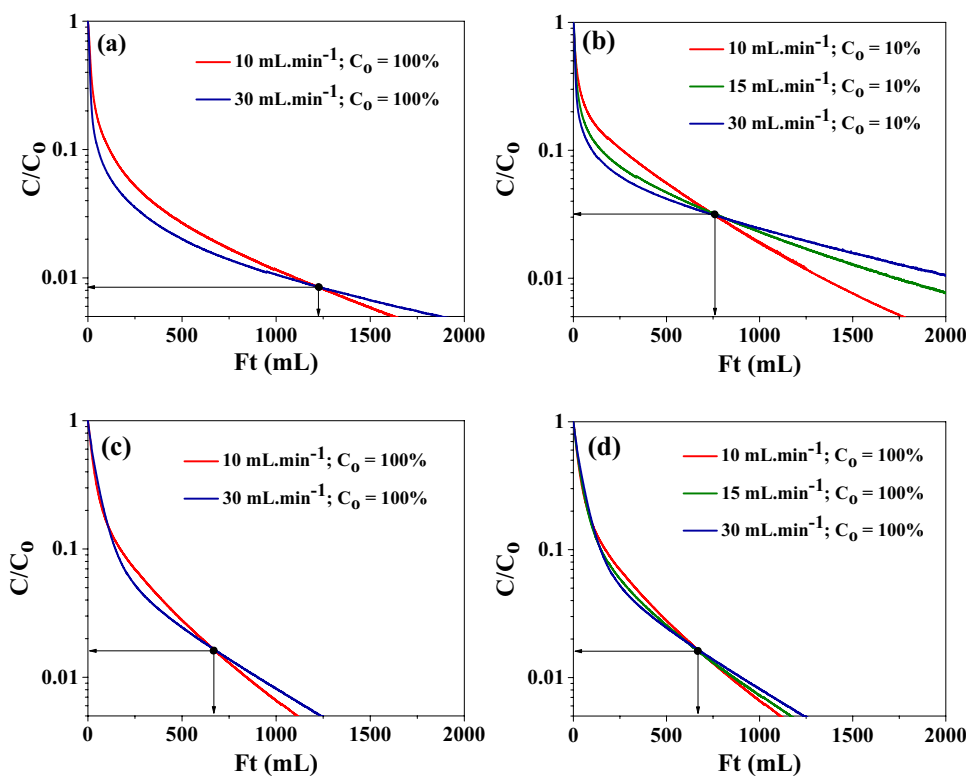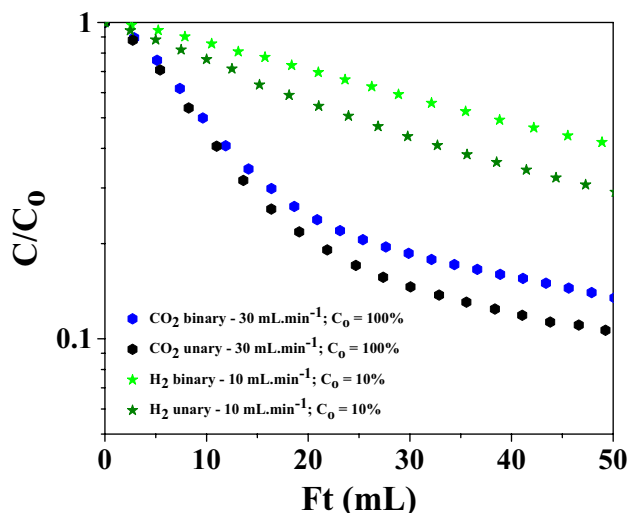
Fig. 5 Binary ZLC profiles of 10% of H_2/He and 100% CO_2 at 90 °C

3.2 Estimation of kinetic parameters

After checking the validity of the experimental methodology and the reliability of the listed operational conditions, we determined the parameters of the ZLC technique and the diffusion characteristics of each adsorbate. However, it is essential to assess if the system is equilibrium- or diffusion-controlled before proceeding. In scenarios characterized by strong adsorption of species and considering the assumption that the ZLC column is not compactly packed – the dead volume is as large as the fluid volume $\left(V_g \cong V_f\right)$ – the value of the parameter γ is very low, and the solution for $\gamma = 0$ can be applied, making the parameter L the maximum non-dimensional concentration gradient within the particle. Furthermore, when the value of L is small ($L < 1$), the adsorbed phase is entirely controlled by equilibrium, as convection is the dominant process in the desorption step. Therefore, a ZLC system targeting this level of L should have flow controllers that allow for low flow rates while maintaining steady-state behavior, even

when larger amounts of adsorbent than usual are applied [6, 12]. On the other hand, when the value of L is large ($L \gg 1$), the process is controlled by the kinetics; hence, it is necessary to conduct experiments at different flow rates to demonstrate which type of regime controls the ZLC system [2, 3]. In circumstances that yield $L > 10$, desorption does not occur under an equilibrium-controlled regime is reached but rather causes the solution value of Eq. (3) to approach the value of π ($\beta_n \rightarrow \pi$) [11]. Consequently, a plot of $\ln(C/C_0)$ versus time generates a long-time asymptotic straight line with an angular coefficient of $\pi^2 D_c/r_c^2$.

The data presented in Table 1 convey trends that were already anticipated regarding the theoretical fundamentals in that diffusivity in the single-component system decreases as the initial concentration of adsorbed gases gets lower and that the diffusivity is higher in single-component systems than in binary-component systems due to the competition of the other species (i.e., competitive desorption). The diffusivity of H_2 dropped by approximately 93% between the single-component system of H_2 ($C_0 = 50\%$) and the 40/60% binary-component system of CO_2/H_2. The diffusivity of CO_2 was reduced by nearly 99% under the same conditions. However, while this signifies a considerable reduction in mass transfer rate, it is not unexpected when considering the specific type of adsorbent and its affinity for CO_2 and H_2. This observation further reveals the behavioral disparities among distinct components of the systems and the influence of the presence of other molecules. It is also important to highlight that the diffusivities obtained in this study (6.36×10^{-5} and 10.64×10^{-5} for unary CO_2 and H_2 gases, respectively, at 293 K) are relatively close to those theoretical values reported by Holden et al. [16] and Camp et al. [9].

The kinetic control over the process was confirmed and defined by the high values of L, which represented the ratio between the diffusion and convective time constants. For instance, the lower threshold range of the L parameter for H_2 in the binary-component system 4/6% of

Table 1 Average values of diffusivity, Henry's constant, and ZLC parameter for CO_2, H_2 and their binary mixtures from the ZLC desorption profiles at 90 °C

Gas/Mixture	$D_c/r_c^2 \times 10^{-2}$ (s^{-1})	D_c (cm^2.s^{-1})	H(dimensionless)	L(dimensionless)
CO_2 *unary*—100%	23.79	1.49×10^{-4}	1.98	25–70
CO_2 *unary*—50%	16.96	1.06×10^{-4}	1.99	33–101
H_2 *unary*—100%	39.79	2.94×10^{-4}	1.30	24–82
H_2 *unary*—50%	31.01	2.33×10^{-4}	1.31	31–93
CO_2 *binary*—40/60% CO_2/H_2	1.33	8.31×10^{-6}	19.21	44–110
CO_2 *binary*—4/6% CO_2/H_2	2.02	1.26×10^{-5}	31.67	18–52
H_2 *binary*—40/60% CO_2/H_2	2.47	1.54×10^{-5}	44.34	18–27
H_2 *binary*—4/6% CO_2/H_2	3.05	1.91×10^{-5}	51.60	13–17

CO_2/H_2 closely approached the range where equilibrium and kinetic properties ($1 < L < 10$) held equal significance in adsorption–desorption processes. This decrease in L as a consequence of D_c increasing was not anticipated when the initial species concentrations of gases are low, especially considering the well-established theoretical principles in such unary-component systems. It is important to note that these ZLC parameters clearly highlight the equilibrium-controlled regime, which would be risky to infer solely from diffusivity values. In other words, even though there was an increase in the diffusion rate of CO_2 and H_2 as their concentrations decreased, this increase was not as significant as the influence of thermodynamic equilibrium in binary systems. Possibly, this rise of diffusivity under these conditions might be caused by the elevated concentration of He gas, which could carry away the recently desorbed molecules.

The binary-component systems studied by the ZLC technique still lack a substantial amount of information to elucidate the trends across various compositions. Another indicative factor pointing towards the necessity of a more profound understanding of binary-component systems is the significant variation in the dimensionless Henry's constant. Table 1 demonstrates that this constant hardly varies in unary-component systems with decreasing initial concentrations of adsorbates, which is in complete accordance with theory.

3.3 Applying kinetic parameters to assess the reliability of the ZLC technique

In recent years, a few studies [6] have presented an illustrative and innovative approach to assess the experimental response of the ZLC technique in comparison with the more traditional method [7] as a consequence of diffusivity and ZLC model parameters valuation.

Figure 6 illustratively depicts the qualitative behavior of unary and binary systems based on the L values observed through the ZLC system. This method of assessment remains independent of concentration and any fine-tuning adjustments made on experimental parameters or by application of correction factors to desorption profiles. The dimensionless time parameter, denoted as τ, represents the ratio of the experimental time to the estimated diffusion rate determined by the particle size squared. The values of the integrals obtained from Eqs. (9) and (10), which are used to calculate the equilibrium phase adsorbed concentration, are inherently linked to the flow rate and consequently the L parameter. An increase in the flow rate corresponds to a decrease in the concentration of the fluid phase, leading to the formation of long-time asymptotes that intersect the profiles obtained from lower flow rates. Therefore, the X-axis of the graphs in Fig. 6 better represents the qualitative assessment of the ZLC system responses, where each pair of curves should always intersect at two distinct points. These points do not necessarily need to coincide with the other profiles, as

Fig. 6 (**a**) The novel plot for a desorption system of CO_2 carried by He. The L values increase in the direction indicated by the arrows. Figure (**c**) is X-axis zoom of figure (**b**), as well as (**b**) is for (**a**), to show a little bit clearly the L parameter increasing in higher relative concentration zone. Different L values indicate different flow rates
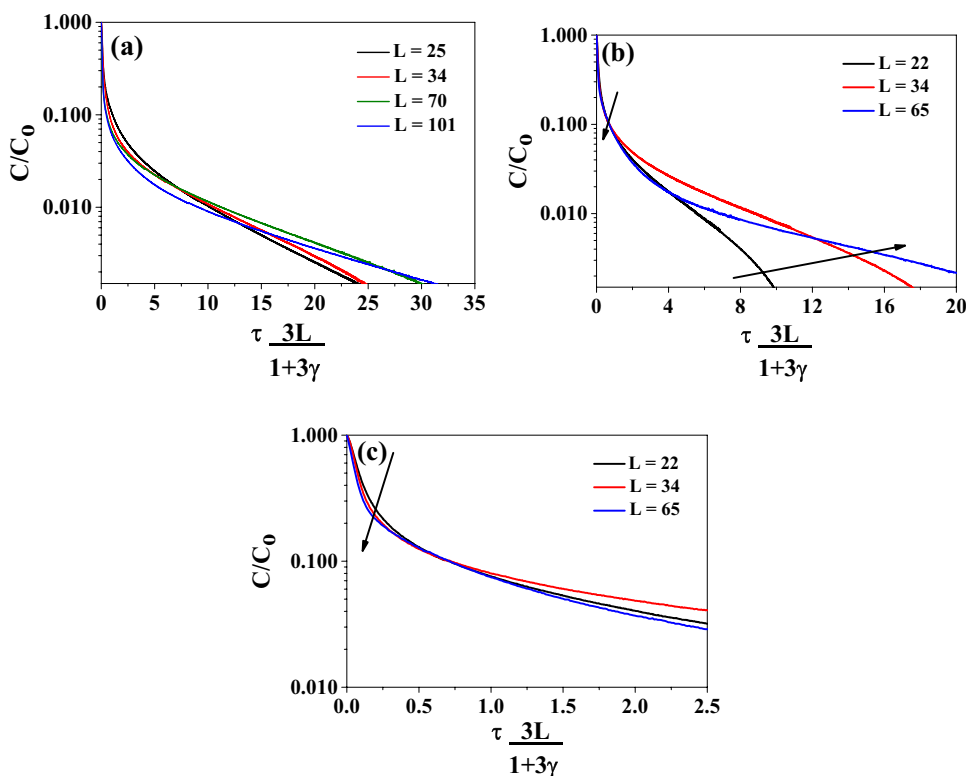
mentioned in the previous section 3.3, and now they form two regions of increasing L values on the graphs.

To ascertain the extent to which the model of equations proposed in this article aligns with the experimental results, an analysis between the L parameter and its corresponding flow rate F can be conducted. For the binary-component system, Table 2 presents the ratio of these two variables, which are closely interconnected, with the value of the lower flow rate serving as the reference. It is evident that these ratios became quite similar in systems with low initial concentrations of CO_2. In the case of H_2, the lack of any significant trend was notable, which can be deemed natural owing to its low adsorption capacity by the POC. This signifies the influence of CO_2 on the diffusion of H_2, as evidenced by the L ratio of 3.29 ($F = 30$ mL.min-1) for a 100% initial concentration in the unary-component system.

3.4 Unary and binary adsorption isotherms

Figure 7 displays equilibrium adsorption isotherms for CO_2 and H_2 single-component systems, obtained from the integrals of ZLC desorption profiles and calculated through Eq. (9). The isotherm data obtained from the volumetric method are also shown, as previously presented in Figure S3. In both cases, the single-component isotherms from the ZLC experiment thoroughly approximate the volumetric data. Hence, the DSL model was fitted to the experimental data obtained from the ZLC method using Eq. (12). In the case of significant differences between the two active adsorption sites; it could be anticipated that those with higher affinity towards the strong species will be predominantly occupied at low-pressure regions, whereas a substantial occupancy of the less favorable active sites will occur only at high pressures.

From the isotherms fitting, the equilibrium constant of Langmuir $b_{CO2;1}$, which describes the adsorbate-adsorbent relationship, and the maximum adsorption capacity $q_{CO2;s1}$

of 'strong' adsorption sites for CO_2 (Fig. 7a) were estimated to be 1.227 bar^{-1} and 2.594 mmol.g^{-1}, respectively, whereas the parameters for the 'weak' sites were $b_{CO2;2}$ = 50.244 bar^{-1} and $q_{CO2;s2}$ = 0.0008 mmol.g^{-1}. For H_2 (Fig. 7b), the equilibrium isotherm parameters were: $b_{H2;1}$ = 0.003 bar^{-1} and $q_{H2;s1}$ = 0.627 mmol.g^{-1}, and $b_{H2;2}$ = 3.141 × 10^{-13} bar^{-1} and $q_{H2;s2}$ = 2.594 × 10^{-6} mmol.g^{-1}. As explained earlier in the methodology section, the parameters of the Langmuir single-component isotherms were used to build binary-component isotherms through Eq. (13). Nevertheless, in practice, only the 'strong' active sites' parameters can be estimated from the single-component isotherms with some degree of confidence, as the experimental data do not reach the high-pressure region that would provide reliable parameters for 'weak' active sites. Figure 7c-d depicts the binary-component system isotherms based on the partial pressure of each component. The trend revealed by the experimental data is qualitatively consistent with that obtained from the theoretical model, thus confirming the alignment between theory and experiment.

Figure 8 illustrates that the amount of adsorbate adsorbed increased upon increasing the pressure. One way to interpret this graph, perhaps the most didactic, is to understand that if there was 0.015 mmol.g^{-1} of adsorbed CO_2 at the beginning of the desorption process, there was also 0.00002 mmol.g^{-1} of H_2 ready to be desorbed, implying that there were about a thousand more molecules of CO_2 'desorbing', thus creating a false impression that CO_2 desorbs faster even though it is more strongly adsorbed. Such an interpretation can only be made appropriately by considering the separation factor in Fig. 9. The weakly-adsorbed component desorbs early in the process, leaving the strongly-adsorbed component to desorb only in the long-time regions. Since the adsorptive affinities of these two components differ significantly, it can be expected that desorption occurs in two distinct stages, with the weak component being removed rapidly with minimal

Table 2 The values of L parameter for binary-component systems

Flow rate, F (mL.min^{-1})	F ratio	L ratio				L			
		CO_2 - 4/6% CO_2/ H_2	CO_2 - 10/15% CO_2/ H_2	CO_2 - 20/30% CO_2/ H_2	CO_2—40/60% CO_2/ H_2	CO_2 - 4/6% CO_2/ H_2	CO_2 - 10/15% CO_2/H_2	CO_2 - 20/30% CO_2/H_2	CO_2—40/60% CO_2/H_2
10	1.00	1.00	1.00	1.00	1.00	17.51	21.85	27.57	48.07
15	1.50	1.48	1.54	1.38	1.51	25.91	33.67	37.91	72.07
30	3.00	2.99	2.96	2.75	2.30	52.40	64.60	75.78	110.36
Flow rate, F (mL.min^{-1})	F ratio	H_2 - 4/6% CO_2/ H_2	H_2 - 10/15% CO_2/H_2	H_2 - 20/30% CO_2/H_2	H_2—40/60% CO_2/H_2	H_2 - 4/6% CO_2/ H_2	H_2 - 10/15% CO_2/H_2	H_2 - 20/30% CO_2/H_2	H_2—40/60% CO_2/H_2
10	1.00	1.00	1.00	1.00	1.00	13.49	16.16	16.89	18.48
15	1.50	1.05	1.21	1.19	1.21	14.11	19.54	20.10	22.35
30	3.00	1.23	1.39	1.46	1.48	16.55	22.48	24.62	27.42

Fig. 7 Single-component isotherms from ZLC desorption profiles at 90 °C for (**a**) CO_2 and (**b**) H_2. Binary-component isotherms from ZLC desorption profiles at 90 °C for (**c**) CO_2 and (**d**) H_2
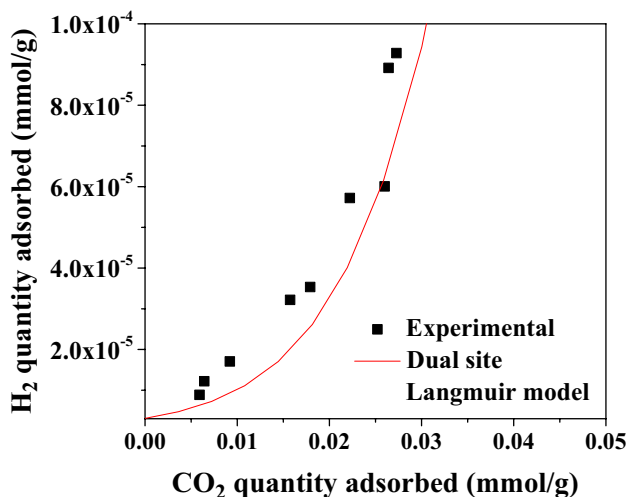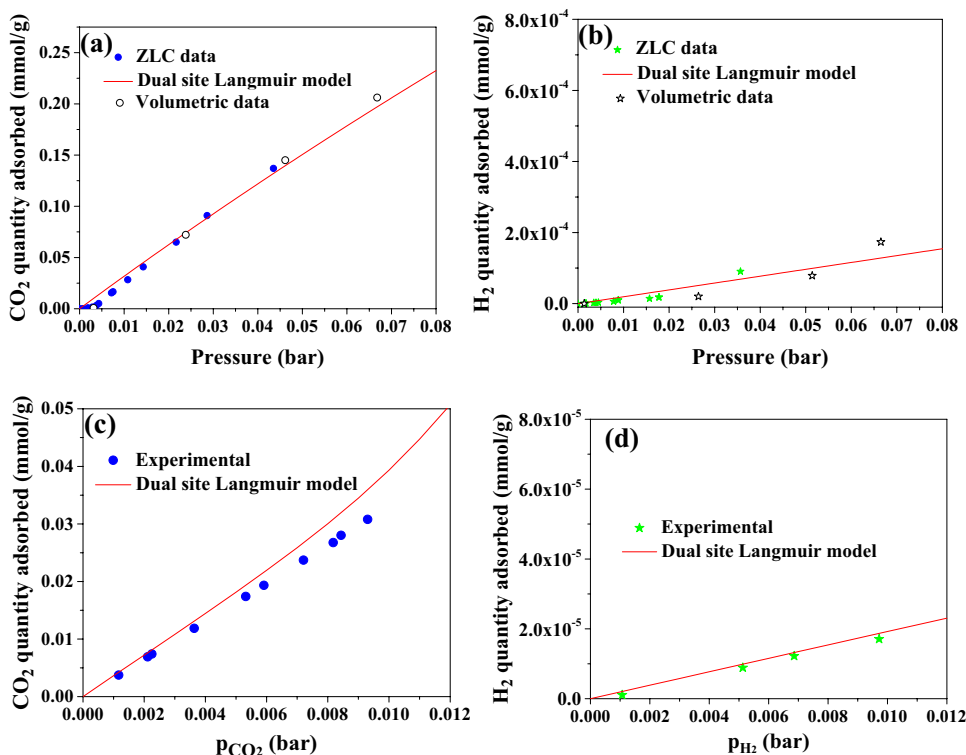

Fig. 8 H_2 and CO_2 adsorbed path of desorption in binary-component system from ZLC desorption profiles at 90 °C
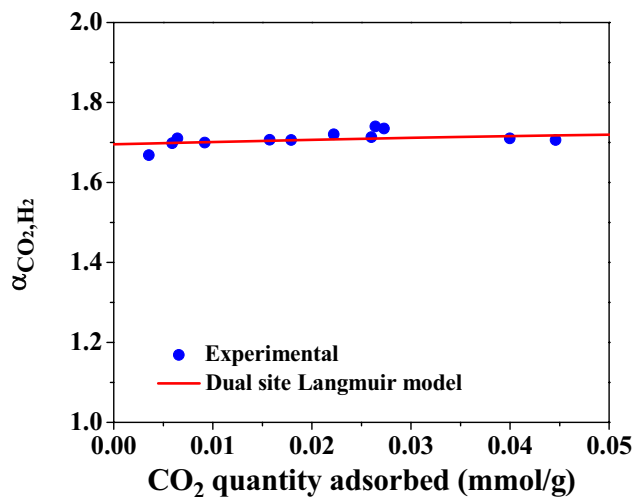
Fig. 9 Separation factor α of the CO_2/H_2 binary-component system versus CO_2 quantity adsorbed perspective from ZLC desorption profiles at 90 °C

variation in the loading of the strong component. Once there is no longer any weak component to be desorbed, the strong component desorbs in a similar fashion as in a single-component system.

In the low-pressure loading limit zone, the separation factor should approach the ratio of Henry's constants for the two components in the binary system. Table 1 presents these constants under two concentration conditions. Dividing H_{H2}

by H_{CO2} gives rise to a ratio of 1.63 for the 4/6% CO_2/H_2 system and 2.21 for the 40/60% CO_2/H_2 system. Once again, the diluted concentration system demonstrated a ratio closer to the values estimated in Fig. 9 by the DSL model. The binary-component isotherms can be analyzed as adsorptive surfaces showing the variation of α as a function of the partial pressure of both studied molecules. In a way, the ZLC

desorption curves produce an intersection among the two surfaces, which is initiated by the equilibrium partial pressure point (at the moment just before desorption starts) and ends at the complete unloading point, with a partial pressure of zero (when complete desorption occurs). However, the path followed in binary-component system is not simply a linear section, even at low concentrations [2]. This is evident from Fig. 8. Therefore, it is necessary to consider the variation of the separation factor with both the concentrations of the adsorbed phases along with the desorption path and the partial loading pressures. In a simplified and approximate manner based on Figs. 7c-d, 8, and 9, it can be stated that at a CO_2 partial pressure of 0.006 bar, there was 0.02 mmol. g^{-1} adsorbed and related with about 0.00003 mmol.g^{-1} of H_2 to be desorbed 1.7 times 'faster' than the CO_2, for instance.

4 Conclusions

In this investigation, we utilized the ZLC technique to determine both the binary adsorption isotherms and kinetic data for CO_2/H_2 systems. The technique was found to be useful in obtaining binary equilibrium data, even in an extremely low-pressure range where numerical values did not precisely match the experimental data. The findings of this study enhance the understanding of operational adjustments and models, rendering the ZLC method readily applicable for binary adsorption measurements at equilibrium. Particularly, it offers a simple way to not only determine the separation factors as a function of pressure but also to measure components' partial isotherms under pure or dilution in a carrier gas atmosphere. Nevertheless, there are clear limitations for the utilization of this technique when choosing operational conditions, adsorbent materials, and gas mixtures. The method's resolution is more satisfactory when the adsorbates' affinities to the adsorbent are neither too similar nor too dissimilar. Consequently, the ZLC technique proves advantageous for more direct and straightforward measurement of separation factors in binary mixtures, as well as for rapidly acquiring kinetic data information. This increases the technique's potential as a valuable tool for a judicious selection of adsorbent materials and process conditions for a particular separation system.

Author contributions Jimmy Moreno: Investigation, Formal analysis, Validation, Writing—review and editing;

Kyle Newport: Data collection;

Ali A. Rownaghi: Conceptualization, Validation, Formal analysis, Supervision, Funding acquisition, Writing—review and editing;

Fateme Rezaei: Conceptualization, Formal analysis, Validation, Supervision, Funding acquisition, Writing – review and editing.

Declarations

References

1. Banat, F., Al-Asheh, S., Al-Lagtah, N.: Adsorptive distillation using molecular sieves and low-cost biobased adsorbents for the break-up of the isopropanol-water azeotrope. Ads. Sci. Tech **21**(9), 821–830 (2003). https://doi.org/10.1260/02636170360744074

2. Brandani, F., Ruthven, D.: Measurement of adsorption equilibria by the zero length column (ZLC) technique part 2: Binary systems. Ind. Eng. Chem. Res. **42**, 1462–1469 (2003). https://doi.org/10.1021/ie020573f

3. Brandani, F., Ruthven, D., Coe, C.G.: Measurement of adsorption equilibrium by the zero length column (ZLC) technique part 1: Single-component systems. Ind. Eng. Chem. Res. **42**, 1451–1461 (2003). https://doi.org/10.1021/ie020572n

4. Brandani, S.: Effects of nonlinear equilibrium on zero length column experiments. Chem. Eng. Sci. **53**, 2791–2798 (1998). https://doi.org/10.1016/S0009-2509(98)00075-X

5. Brandani, S.: A simple graphical check of consistency for zero length column desorption curves. Chem. Eng. Technol. **39**, 1194–1198 (2016). https://doi.org/10.1002/ceat.201500634

6. Brandani, S., Mangano, E.: The zero length column technique to measure adsorption equilibrium and kinetics: lessons learnt from 30 years of experience. Adsorption **27**, 319–351 (2021). https://doi.org/10.1007/s10450-020-00273-w

7. Brandani, S., Ruthven, D.M.: Analysis of ZLC desorption curves for liquid systems. Adsorption **50**, 2055–2059 (1995). https://doi.org/10.1007/BF00127043

8. Briggs, M.E., Cooper, A.I.: A perspective on the synthesis, purification, and characterization of porous organic cages. Chem. Mat. **29**(1), 149–157 (2017). https://doi.org/10.1021/acs.chemmater.6b02903

9. Camp, J.S., Sholl, D.S.: Transition state theory methods to measure diffusion in flexible nanoporous materials: application to a porous organic cage crystal. J. Phys. Chem. C **120**, 1110–1120 (2016). https://doi.org/10.1021/acs.jpcc.5b11111

10. Chen, J., Loo, L.S., Wang, K.: An ideal absorbed solution theory (IAST) study of adsorption equilibria of binary mixtures of methane and ethane on a templated carbon. J. Chem. Eng. Data **56**, 1209–1212 (2011). https://doi.org/10.1021/je101099c

11. Eic, M., Ruthven, D.M.: A new experimental technique for measurement of intracrystalline diffusivity. Zeolites **8**, 40–45 (1988). https://doi.org/10.1016/S0144-2449(88)80028-9

12. Friedrich, D., Mangano, E., Brandani, S.: Automatic estimation of kinetic and isotherm parameters from ZLC experiments. Chem. Eng. Sci. **126**, 616–624 (2015). https://doi.org/10.1016/j.ces.2014.12.062

13. Gelles, T., Rezaei, F.: Diffusion kinetics of CO_2 in amine-impregnated MIL-101, alumina, and silica adsorbents. AIChE J. **66**, 1–15 (2020). https://doi.org/10.1002/aic.16785

14. Gelles, T., Rownaghi, A.A., Rezaei, F.: Diffusion kinetics of CO_2, CH_4, and their binary mixtures in porous organic cage CC3. J. Phys. Chem. C. **123**, 24172–24180 (2019). https://doi.org/10.1021/acs.jpcc.9b07438

15. Giraldo, L., Rodriguez-Estupiñán, P., Moreno-Piraján, J.C.: Isosteric heat: Comparative study between Clausius-Clapeyron, CSK and adsorption calorimetry methods. Processes **7**(4),(2019). https://doi.org/10.3390/pr7040203

16. Holden, D., Jelfs, K.E., Trewin, A., Willock, D.J., Haranczyk, M., Cooper, A.I.: Gas diffusion in a porous organic cage: Analysis of dynamic pore connectivity using molecular dynamics simulations. J. Phys. Chem. C **118**, 12734–12743 (2014). https://doi.org/10.1021/jp500293s

17. Hu, X., Mangano, E., Friedrich, D., Ahn, H., Brandani, S.: Diffusion mechanism of CO_2 in 13X zeolite beads. Adsorption **20**, 121–135 (2014). https://doi.org/10.1007/s10450-013-9554-z

18. Kärger, J., Ruthven, D.M., Theodorou, D.N.: Sorption Kinetics. In: Diffusion in Nanoporous Materials, pp. 143–189. John Wiley & Sons, Ltd (2012). https://doi.org/10.1002/9783527651276.ch6

19. Kerry, F.G.: Industrial Gas Handbook: Gas Separation and Purification, 1st edn. CRC Press (2007). https://doi.org/10.1201/9781420008265

20. Krishnan, K., Crawford, J.M., Thallapally, P.K., Carreon, M.A.: Porous organic cages CC3 and CC2 as adsorbents for the separation of carbon dioxide from nitrogen and hydrogen. Ind. Eng. Chem. Res. **61**, 10547–10553 (2022). https://doi.org/10.1021/acs.iecr.2c00146

21. Maqsood, K., Mullick, A., Ali, A., Kargupta, K., Ganguly, S.: Cryogenic carbon dioxide separation from natural gas: A review based on conventional and novel emerging technologies. Rev. Chem. Eng. **30**, 453–477 (2014). https://doi.org/10.1515/revce-2014-0009

22. Ruthven, D., Brandani, F.: ZLC response for systems with surface resistance control. In: Adsorption, vol. 11, pp. 31–34. (2005). https://doi.org/10.1007/s10450-005-1090-z

23. Ruthven, D.M., Vidoni, A.: ZLC diffusion measurements: Combined effect of surface resistance and internal diffusion. Chem. Eng. Sci. **71**, 1–4 (2012). https://doi.org/10.1016/j.ces.2011.11.040

24. Shade, D., Bout, B.W.S., Sholl, D.S., Walton, K.S.: Opening the toolbox: 18 experimental techniques for measurement of mixed gas adsorption. Eng. Chem. Res **61**(14), 2367–2391 (2022). https://doi.org/10.1021/acs.iecr.1c03756

Authors and Affiliations

Jimmy D. L. Moreno[2] · **Kyle Newport**[3] · **Ali A. Rownaghi**[4] · **Fateme Rezaei**[1]

✉ Fateme Rezaei
rezaeif@miami.edu

1 Department of Chemical, Environmental and Materials Engineering, University of Miami, Miami, FL 33124, USA

2 Grupo de Pesquisa Em Separações Por Adsorção (GPSA), Departamento de Engenharia Química, Universidade Federal Do Ceará, Campus Do Pici, Bl. 709, Fortaleza 60455-760, Brazil

3 Linda and Bipin Doshi Department of Chemical and Biochemical Engineering, Missouri University of Science and Technology, Rolla, MO 65409-1230, USA

4 National Energy Technology Laboratory (NETL), United States Department of Energy, Pittsburgh, PA 15236, USA